Chinese Chemical Letters 35 (2024) 109271

Contents lists available at ScienceDirect

Chinese Chemical Letters

journal homepage: www.elsevier.com/locate/cclet

Novel P-doping-tuned Pd nanoflowers/S,N-GQDs photo-electrocatalyst for high-efficient ethylene glycol oxidation

Xiaoxiao Huang[a], Zhi-Long He[a], Yangpeng Chen[a], Lei Li[b,*], Zhenyu Yang[b], Chunyang Zhai[a,*], Mingshan Zhu[c]

[a] School of Materials Science and Chemical Engineering, Ningbo University, Ningbo 315211, China
[b] College of Biological, Chemical Sciences and Engineering, Jiaxing University, Jiaxing 314001, China
[c] Guangdong Key Lab oratory of Environmental Pollution and Health, School of Environment, Jinan University, Guangzhou 510632, China

ARTICLE INFO

Article history:
Received 7 July 2023
Revised 16 October 2023
Accepted 31 October 2023
Available online 4 November 2023

Keywords:
Non-metallic P–doping
Sulfur nitrogen co-doped graphene quantum dots
Pd nanoflowers
Photo-electrocatalytic
Ethylene glycol oxidation

ABSTRACT

Traditional photo-electcatalyst structures of small noble metal nanoparticles assembling into large-scale photoactive semiconductors still suffer from agglomeration of noble metal nanoparticles, insufficient charge transfer, undesirable photoresponse ability that restricted the photo-electrocatalytic performance. To this end, a novel design strategy is proposed in this work, namely integrating small-scale photoactive materials (doped graphene quantum dots, S,N-GQDs) with large-sized noble metal (PdP) nanoflowers to form novel photo-electrocatalysts for high-efficient alcohol oxidation reaction. As expected, superior electrocatalytic performance of PdP/S,N-GQDs for ethylene glycol oxidation is acquired, thanks to the nanoflower structure with larger specific surface area and abundant active sites. Furthermore, nonmetal P are demonstrated, especially optimizing the adsorption strength, enhancing the interfacial contact, reducing metal agglomeration, ensuring uniform and efficient doping of S,N-GQDs, and ultimately significantly boost the catalytic activity of photo-electrocatalysts.

Direct liquid fuel cells (DAFCs), compared with traditional fossil fuels, can completely convert the contained chemical energy into mechanical energy, whose efficiency is not limited by the Kano cycle [1–3]. Moreover, solar energy is a kind of renewable green energy source. Therefore, the effective combination of DAFCs with solar energy using photoelectrocatalytic technology can increase the utilization of energy [4,5]. Regrettably, several challenges such as insufficient reaction kinetics and toxic effects of intermediate products still limit the practical application of photo-electrolytic technology [6]. To this end, the rational design and development of more efficient and stable photoelectcatalysts are crucial [7,8]. At present, abundant photoelectcatalysts are constructed through depositing noble metal nanoparticles onto some large-sized photoactive materials (*e.g.*, nanotubes, nanowires, and nanosheet) [9,10]. Unfortunately, the lack of neighboring coordinating atoms on the metal nanoparticles surface, the high surface energy that predisposes them to agglomeration make the catalytic activity and lifetime of photoelectcatalysts greatly reduced [11–15]. To this end, a novel design method, assembling small-sized photoactive materials into large-sized noble metal nanocatalysts could (1) significantly elevate the degree of light response; (2) substantially boost charge transfer efficiency is able; (3) make full use of precious metals, thereby acquiring superior photo-electrocatalytic performance.

In view of that, precise design and rational regulation of metal nanostructures and small-sized photoactive semiconductors are essential. Among numerous large-sized nanostructures, three-dimensional freestanding nanoflowers with abundant active sites, large specific surface area, and convenient tuning of electronic structures can efficaciously promote the sufficient contact of catalysts with active molecules, with promising applications [16–20]. Sulfur-nitrogen-doped graphene quantum dots (S,N-GQDs) are a new zero-dimensional carbon material with high visible light absorption capacity and adjustable Fermi energy level, which can be used as electron transport medium and photosensitizer, inducing efficient separation of electron-hole pairs, thereby improving catalytic performance [21–23]. Therefore, noble metal nanoflowers combined with S,N-GQDs can construct a novel and more efficient photoelectcatalyst.

In addition, the appropriate interaction force between the two is essential to optimize the adsorption strength and reduce agglomeration to ensure the uniform and availably doping of S,N-GQDs onto noble metal nanoflowers. Studies [24–27] have shown

* Corresponding authors.
E-mail addresses: leili@mail.zjxu.edu.cn (L. Li), zhaichunyang@edu.nbu.cn (C. Zhai).

https://doi.org/10.1016/j.cclet.2023.109271
1001-8417/

that combination of nonmetal elements and noble metals can modulate the electronic structure of noble metal, modify the noble metal surface, and thus properly enhance the interaction. This is due to the high electronegativity of nonmetal elements, especially phosphorus atoms, easily polarize the surrounding atoms and thus can change the density of electron clouds [28,29]. At the same time, nonmetal elements can form more chemical bonds with heteroatom doped carbon-based materials, which further reinforce the interaction [30,31].

Different from the traditional photoelectcatalyst design concept, in this work, a novel PdP/S,N-GQDs photoelectcatalyst was constructed by combining a small photoactive material with noble metal nanoflower, as shown in Scheme S1 (Supporting information). Interestingly, the PdP/S,N-GQDs exhibited the best photoelectrocatalytic activity and durability, consistent with the expected results. This work confirms that small-sized photoactive materials combine with large-sized noble metal nanomaterials is a rather efficient way to construct novel and efficient photoanode catalysts and provides a new avenue for the rational design of visible light assisted fuel cell anode catalysts in the future.

SEM, TEM, and EDX were used to explore the morphology, structure of the prepared catalysts. The SEM (Figs. 1A and B) and TEM (Figs. 1C and D) results display that Pd and PdP nanoflowers were assembled through a large number of nanosheets and the addition of P elements and S,N-GQDs did not affect the structure and morphology of catalysts. It can also be clearly observed that S,N-GQDs were well dispersed on the surface of PdP nanoflowers. Furthermore, the lattice size and crystal plane arrangement of PdP and PdP/S,N-GQDs studied by high-resolution TEM. It is calculated that the lattice spacing of PdP is about 0.22 nm (Fig. 1E), corresponding to the crystal plane of PdP (111) [32,33]. Moreover, the lattice spacing of S,N-GQDs was about 0.25 nm (Fig. 1F), corresponding to the S,N-GQDs [22,34]. Furthermore, in the obtained PdP/S,N-GQDs sample, the corresponding element mapping indicated the existence of C, N, O, P, S, and Pd elements in the sample (Fig. 1G).

The crystal structures of the samples were investigated by XRD. As presented in Fig. 2A, the diffraction peaks of as prepared samples are matched with the crystal planes of Pd face-centered cubic (FCC) [34]. Howbeit, the characteristic peaks of P and S,N-GQDs are not be observed, which is due to the absence of crystal structure of S,N-GQDs and low P content, respectively.

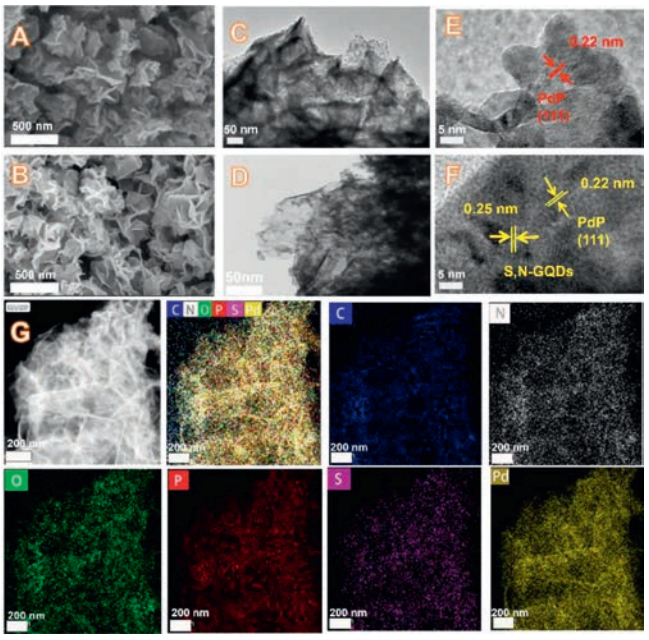

Fig. 1. SEM images of (A) Pd and (B) PdP. TEM and HRTEM images of (C, E) PdP and (D, F) PdP/S,N-GQDs. (G) TEM-EDX mapping of PdP/S,N-GQDs.

Fig. 2B exhibits the C 1s XPS (X-ray photoelectron spectroscopy) high-resolution spectra of PdP/S,N-GQDs and Pd/S,N-GQDs, four major peaks at 284.8, 285.5, 286.5 and 288.2 eV are found, which belong to C=C, C-S/C–N, C–O, and C=O, respectively [35]. The large contributions of C=C and C–N/C-S indicate that structure of the graphite matrix is mainly composed of C-bonded and there is a strong interactions between S and N atoms, while C–O and C=O are mainly assigned to carboxylate groups or carbonyl [36]. The P 2p spectrum in Fig. 2C showed the P element within the PdP/S,N-GQDs. Meanwhile, strong P-S and P-N convolution peak can be clearly observed, indicating the exsitence of chemical bonds between P and S, N [37]. Figs. 2D and E display S 2p and N 1s XPS spectra of the samples. As for the S 2p XPS spectrum of Pd/S,N-GQDs, four peaks are assigned to S-N, S-Pd, and S-O, respectively. The three characteristic peaks of N 1s XPS spectra of Pd/S,N-GQDs belong to N-Pd, C–N-C, and N–H, respectively. When nonmetal P was introduced, it was found that convoluted peaks of S-P and N-P at 163.3 eV and 399.3 eV, respectively, which strongly evidenced that P can enhance the interaction force [38]. As shown in Fig. 2F, the Pd 3d XPS spectrum of PdP/S,N-GQDs show peaks at 337.3 eV and 342.5 eV, 335.6 eV and 340.8 eV are attributed to the Pd $3d_{3/2}$ and Pd $3d_{5/2}$ of Pd(II) and Pd(0), respectively. Evidently, the peak of Pd(0) is obviously higher than that of Pd(II), manifesting that most Pd atoms are reduced and Pd(0) dominates in the reaction environment [38]. Interestingly, the Pd 3d deconvolution peak position of PdP/S,N-GQDs electrode was negatively shifted compared with pure Pd, which confirmed the existence of charge transfer and interaction between PdP and S,N-GQDs.

It is well known that one of the important indicators to evaluate the catalytic performance of catalysts is the electrochemically active surface area (ECSA). The ECSA of the catalysts was calculated from the hydrogen adsorption/desorption peak region on the CV (cyclic voltammetry) curve in Fig. S1 (Supporting information). From the calculations, the ECSA values of PdP/S,N-GQDs (1388.55 cm^2/mg), Pd/S,N-GQDs (658.73 cm^2/mg), PdP (30.27 cm^2/mg), and Pd (3.17 cm^2/mg) electrodes, respectively. Undoubtedly the PdP/S,N-GQDs electrode has the largest ECSA value, which means that the PdP/S,N-GQDs electrodes had more active sites as well as higher catalytic performance.

The photoelectrocatalytic performance of the samples was evaluated by the oxidation reaction of ethylene glycol. Among them, the catalytic performance of the prepared catalysts was evaluated by CV tests (Fig. 3) under different conditions. Firstly, the GCE has no impact on the measurements of catalytic performance of electrode materials (Fig. S2 in Supporting information). It is well known that the positive sweep curve peak current density (I_p) is a standard indicator to measure the catalytic performance of electrodes [25]. As shown Fig. 3A, it can be clearly observed that the PdP electrode has a significantly higher positive oxidation peak than pure Pd electrode. After modification by S,N-GQDs, the I_p of PdP/S,N-GQDs is not only higer than PdP electrode, but also higher than PdP/GQDs. When visible light was introduced, as displayed in Fig. 3C, the I_p continued to increase and reached 18.5 A/mg_{Pd}, which was 3.1 and 5.2 times higher than that of Pd/S,N-GQDs and PdP/GQDs under the same condition, respectively. Meanwhile, to facilitate the observation, the areal activity and mass activity of catalytic oxidation of ethylene glycol with different electrodes were examined, as depicted in Figs. 3B and D. Impressively, the above results demonstrated that PdP/S,N-GQDs electrode possessed excellent performance of EGOR, which was much higher than that of the previously reported EGOR photoelectcatalysts (Fig. 3E) [18,39-43]. The results showed that the introduction of nonmetal P and the modification of S,N-GQDs greatly increased the charge trans-

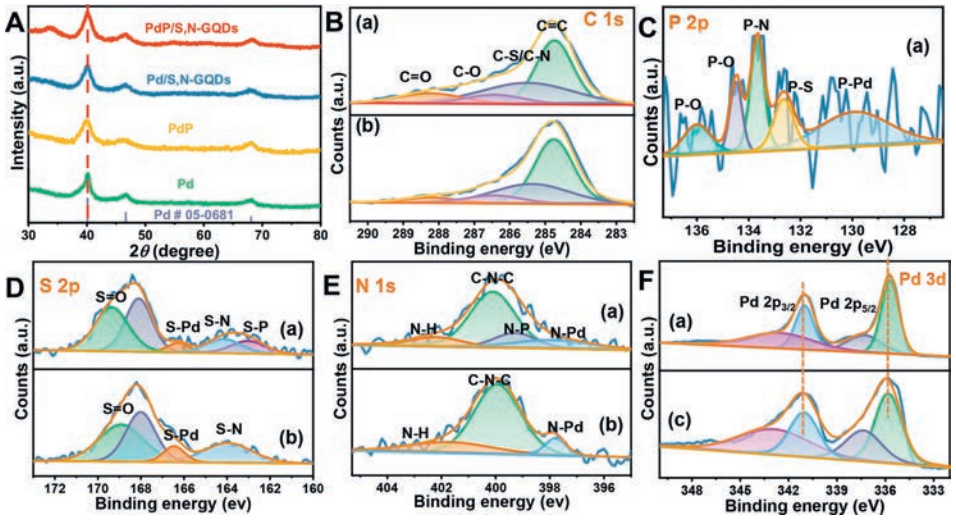

Fig. 2. (A) XRD patterns of different catalysts. XPS high-resolution survey of (B) C 1s, (C) P 2p, (D) S 2p, (E) N 1s, (F) Pd 3d of (a) PdP/S,N-GQDs, (b) Pd/S,N-GQDs, and (c) pure Pd.

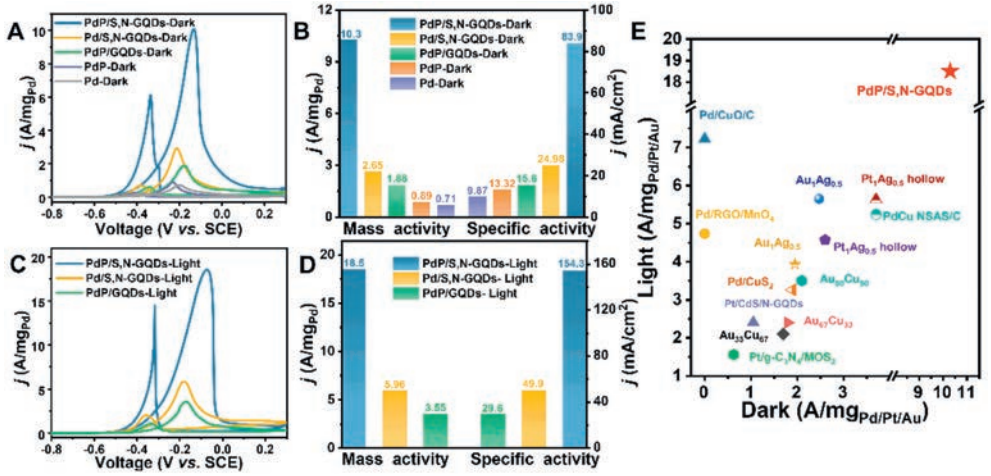

Fig. 3. (A, C) CV curves of different electrodes without and with visible light irradiation in 1.0 mol/L EG + 1.0 mol/L KOH solution at a scan rate of 50 mV/s. (B, D) The histogram of mass and specific activities of the electrodes. (E) EGOR performance of PdP/S,N-GQDs and reported photoelectrocatalysts for comparison in alkalinity electrolyte.

fer efficiency of the catalysts, decreased the photoelectron hole recombination rate, and significantly improved the catalytic oxidation ability of the PdP/S,N-GQDs composite electrodes.

From an application perspective, toxicity resistance and long-term durability are also essential criteria for evaluating catalysts. Accordingly, CP and *I-t* were measured to evaluate the toxicity resistance and durability of the catalysts. The anti-toxic ability of the catalysts was judged by the length of polarization time, *i.e.*, longer polarization times indicate better resistance to toxicity [44]. As displayed in Fig. 4A, PdP/S,N-GQDs electrodes displayed the longest polarization times under dark condition compared to other electrodes. The duration of PdP/S,N-GQDs electrode reached up to 8846 s when visible light was introduced, which was 2.15 times longer than that under dark condition, illustrating that the visible light assisted PdP/S,N-GQDs catalyst exhibited excellent anti-toxic ability. Subsequently, *I-t* experiments were used to test the stability of the samples, as shown in Fig. 4B, the results showed that the mass activity of PdP/S,N-GQDs under dark conditions was higher than other catalysts in the dark, which was 10.4, 35.2, and 55.6 times higher than that of Pd/S,N-GQDs, PdP, and the Pd, respectively, after 3600 s. Moreover, the stability of the PdP/S,N-GQDs electrode was further boosted when visible light was introduced, with a mass activity as high as 884.9 mA/mg_{Pd}. The above phenomena illustrated that PdP/S,N-GQDs composite electrodes exhibited much better anti-toxicity ability, and durability under the assistance of visible light compared with Pd/S,N-GQDs, PdP, and Pd electrodes.

To examine the response capability of the samples to visible light, transient photoresponse curves were acquired, as depicted in Fig. 4C. The results showed that the photocurrent density of PdP/S,N-GQDs reached 432.4 mA/mg_{Pd}, which was 3.55 times higher than that of Pd/S,N-GQDs. The higher photocurrent response confirmed the efficient transfer and separation of photogenerated electron-hole pairs in PdP/S,N-GQDs electrodes. This is due to that the addition of nonmetal P can effectually regulate the electronic structure, thus facilitating the separation of photogenerated electron-hole pairs [36,45]. Furthermore, during the on/off cycle, the responding photocurrent appeared repeatedly, which further proved that the catalysts possessed strong stability and anti-toxic ability.

The charge mobility of the interface between these electrodes in the presence and absence of visible light was further investigated using EIS tests. It is well known that the smaller the impedance arc radius, the faster the charge transfer [37]. The EIS spectra of PdP/S,N-GQDs electrodes at various potentials were measured in alkaline electrolyte solution, as shown in Fig. S3 (Sup-

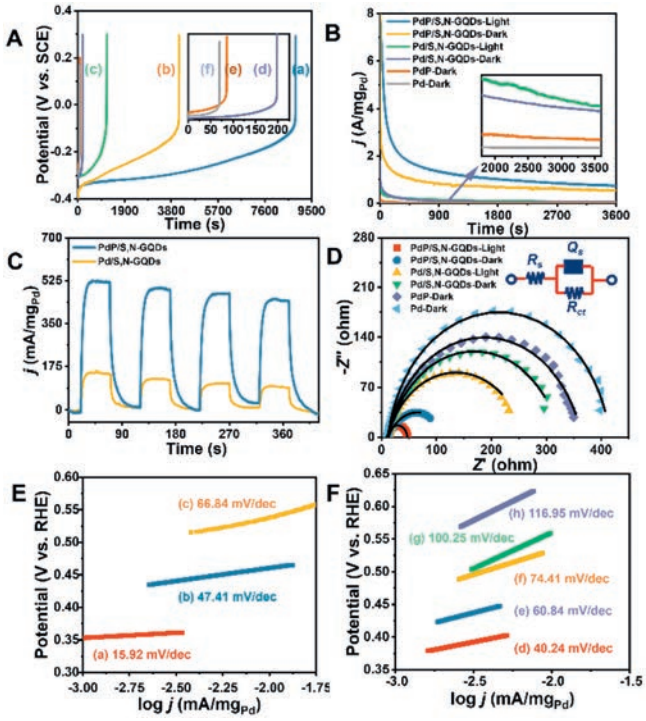

Fig. 4. (A, B) CP curves and *I-t* curves of (a, b) PdP/S,N-GQDs, (c, d) Pd/S,N-GQDs, (e) PdP, and (f) Pd electrodes with and without visible light illumination. (C) Photocurrent response curves of the samples. (D) Nyquist diagram of the different electrodes under light and dark conditions. (E, F) Tafel curve slopes of (a, d) PdP/S,N-GQDs, (b, e) Pd/S,N-GQDs (c, f), PdP/GQDs, (g) PdP, and (h) Pd with and without visible light in 1.0 mol/L EG + 1.0 mol/L KOH solution.

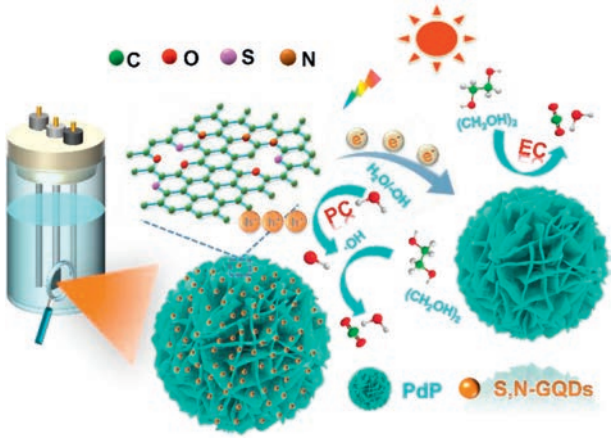

Fig. 5. Proposed the mechanism of photoelectrocatalytic oxidation of glycol alcohol by PdP/S,N-GQDs electrode under the assistance of visible light.

porting information). It is known from the figure that the potential of the smallest arc radius of PdP/S,N-GQDs electrode is −0.2 V under both light and dark conditions, indicating faster interfacial charge migration at this potential. Consequently, the potential of the EIS spectra test of different electrodes was at −0.2 V, as shown in Fig. 4D, the variation trend of impedance was similar to the *I-t* performance of the samples. The samllest arc radius (R_{ct}) was obtained when the PdP/S,N-GQDs electrode was irradiated under visible light, indicating that visible light illumination decreases their electron transfer resistance and thus increases the interfacial charge electron transfer rate. To display the charge transfer resistance parameters intuitively, the EIS spectra were fitted with the equivalent circuits. Where R_s, R_{ct}, and Q_s represent the electrolyte resistance, charge transfer resistance, and constant phase element (CPE), respectively [38]. Table S1 (Supporting information) summarizes the numerical size of Rct of the different samples. The results show that the separation efficiency of the photogenerated electron hole pairs, as well as the interfacial charge transfer rate of the PdP/S,N-GQDs composite electrodes, are greatly enhanced compared with those of the other electrodes, which can greatly increase the catalytic performance. In addition, to further probe the charge migration characteristics as well as the oxidation kinetic characteristics of the catalysts, LSV tests, and the corresponding Tafel slopes were performed, as displayed in Figs. 4E and F. The LSV curves (Fig. S4 in Supporting information) show that the PdP/S,N-GQDs electrode has a lower onset potential and higher current density compared with other electrodes under dark conditions, and this result is consistent with the above CV. Moreover, the onset potential of the PdP/S,N-GQDs electrode under visible light conditions was further negatively shifted, and the current density increased somewhat, much higher than that of the Pd/S,N-GQDs, and PdP/ GQDs electrodes under light condition. Meanwhile, the Tafel slope curves of catalysts were calculated from the Tafel equation and fitted curves. It is well known that the faster the kinetic speed of the catalytic reaction, that is, the smaller the Tafel slope. As can be seen from Fig. 4F, PdP/S,N-GQDs (40.24 mV/dec) possessed much smaller Tafel slopes compared with those of Pd/S,N-GQDs (60.84 mV/dec), PdP/GQDs (74.41 mV/dec), PdP (100.25 mV/dec), Pd (116.95 mV/dec) under dark conditions. When visible light was introduced (Fig. 4E), the Tafel slope of PdP/S,N-GQDs was further reduced to 15.92 mV/dec, which was smaller than that of Pd/S,N-GQDs (47.41 mV/dec), PdP/GQDs (66.84 mV/dec). The above phenomena indicated that the PdP/S,N-GQDs electrode exhibited higher charge mobility and better oxidation kinetic rate under the assistance of visible light.

Obviously, the PdP/S,N-GQDs electrode demonstrates remarkable catalytic performance, excellent stability, and potent antivirulence ability under visible light assistance. The proposed mechanism for ethylene glycol oxidation involves two distinct processes: electrocatalysis and photocatalysis, as illustrated in Fig. 5. The mechanism was analyzed by XPS, revealing that the Pd 3d deconvolution peak position of the PdP/S,N-GQDs electrode was negatively shifted compared to pure Pd, confirming the existence of charge transfer and interaction between PdP and S,N-GQDs. When nonmetal P was introduced, it was able to find convoluted peaks S-P and N-P at 163.3 eV and 399.3 eV, respectively, which was compelling evidence that P can enhance the interaction force. Furthermore, the nanoflower structure assembled from nanoflakes of PdP/S,N-GQDs composite catalysts provides a larger specific surface area and more active sites, thereby facilitating catalytic reactions. Consequently, the electrocatalytic properties of the catalysts were significantly augmented.

Under visible light conditions, the S,N-GQDs generate a great number of photogenerated electrons that rapidly transfer to the surface of PdP nanoflowers, resulting in improved electron-hole separation efficiency. However, the photo-generated holes exhibit robust oxidative properties and can oxidize H_2O/OH^- to form active superoxide hydroxyl radicals (•OH). Then •OH further oxidizes organic small molecules such as ethylene glycol adsorbed on the surface of catalyst to form a photo-assisted catalytic process. As a result, the catalytic effect of PdP/S,N-GQDs on ethylene glycol is significantly enhanced under visible light assistance. The electrocatalytic and photo-catalytic specific pathways are presented in the supporting information.

In this paper, a novel approach involving the assembly of small-scale photoactive materials into large-scale noble metal nanoflowers has been developed to create innovative photo-electrocatalysts (PdP/S,N-GQDs) for highly efficient ethylene glycol oxidation reac-

tions. Remarkably, the PdP/S,N-GQDs photo-electrocatalyst exhibits exceptional catalytic activity, resistance to toxicity, and long-term stability. which is due to the increased photo-response intensity and the accelerated electron-holes separation *via* the introduction of S,N-GQDs. Furthermore, the essential incorporation of nonmetal P not only effectively tunes the electronic structure and generates a large number of defects but also creates numerous additional active sites. It can also reinforce the interaction force between Pd and S,N-GQDs to make it uniform and effectively doped. This study provides a rational strategy to design the photo-electrocatalysts materials for anodes in DAFCs.

Declaration of competing interest

The authors declare that they have no known competing financial interests or personal relationships that could have appeared to influence the work reported in this paper.

Acknowledgments

This work was supported by Zhejiang Provincial Natural Science Foundation of China (No. LTGS23B030002) and the National Natural Science Foundation of China (Nos. 21978111 and 22278175).

Supplementary materials

Supplementary material associated with this article can be found, in the online version, at doi:10.1016/j.cclet.2023.109271.

References

[1] Q. Chen, C. Yuan, C. Zhai, Chin. Chem. Lett. 33 (2022) 983–986.
[2] M. Yang, M. Pang, J. Chen, et al., ACS Appl. Mater. Interfaces 13 (2021) 9830–9837.
[3] C.P. Deming, R. Mercado, J.E. Lu, et al., ACS Sustain. Chem. Eng. 4 (2016) 6580–6589.
[4] L. Zhu, Y. Liang, L. Sun, et al., Inorg. Chem. 60 (2021) 10707–10714.
[5] Y. He, K. Chen, M.K.H. Leung, et al., Chem. Eng. J. 428 (2022) 131074.
[6] Y. Zhao, J. Ning, X. Hu, et al., Appl. Surf. Sci. 505 (2020) 144488.
[7] J. Deng, Y. Su, D. Liu, et al., Chem. Rev. 119 (2019) 9221–9259.
[8] A. Parastaev, V. Muravev, E.Huertas Osta, et al., Nat. Catal. 3 (2020) 526–533.
[9] L. Cheng, C. Zhang, Y. Liu, J. Am. Chem. Soc. 141 (2019) 16296–16302.
[10] X. Zhang, L. Han, H. Chen, Chin. Chem. Lett. 33 (2022) 1117–1130.
[11] S. He, C. Yan, X.Z. Chen, et al., Appl. Catal. B 276 (2020) 119138.
[12] X. Huang, Z.L. He, Y. Chen, et al., J. Colloid Interface Sci. 625 (2022) 850–858.
[13] F. Gao, Y. Zhang, F. Ren, et al., Adv. Funct. Mater. 30 (2020) 2000255.
[14] S. Huang, T. Ouyang, B.F. Zheng, M. Dan, Z.Q. Liu, Angew. Chem. Int. Ed. 60 (2021) 9546–9552.
[15] J. Zhang, P. Tian, A. Xu, et al., Chin. Chem. Lett. 34 (2023) 108446.
[16] W. Su, R. Sun, F. Ren, et al., Appl. Surf. Sci. 491 (2019) 735–741.
[17] B. Li, C. Lai, M. Zhang, et al., Chem. Eng. J. 409 (2021) 128281.
[18] Z.L. He, C. Yuan, H. Gao, et al., ACS Sustain. Chem. Eng. 8 (2020) 12331–12341.
[19] S. Huang, B.F. Zheng, Z.Y. Tang, et al., Chem. Eng. J. 422 (2021) 130086.
[20] J. Xu, J. Ma, Y. Peng, et al., Chin. Chem. Lett. 34 (2023) 107527.
[21] C. Feng, Y. Deng, L. Tang, et al., Appl. Catal. B 239 (2018) 525–536.
[22] D. Zhang, S. Yang, X. Fang, Chin. Chem. Lett. 33 (2022) 4669–4674.
[23] H. Xie, C. Hou, H. Wang, Nanoscale Res. Lett. 12 (2017) 400.
[24] Z. Li, R. Wu, L. Zhao, et al., Nano Res. 14 (2021) 3795–3809.
[25] C. Hernandez Mejia, T.W. van Deelen, K.P. de Jong, Nat. Commun. 9 (2018) 4459.
[26] S. Huang, F. Feng, R.T. Huang, et al., Adv. Mater. 34 (2022) 2208438.
[27] W. Yan, M. Zheng, P. Chuang, et al., Chin. Chem. Lett. 34 (2023) 108021.
[28] Z. Li, X. Lu, J. Teng, et al., Nanoscale 13 (2021) 11314–11324.
[29] G. Su, S. Yang, Y. Jiang, et al., Prog. Surf. Sci. 94 (2019) 100561.
[30] Q. Chen, C. Yuan, Z. He, et al., Mikrochim Acta 189 (2022) 208.
[31] C.T. Selepe, S.S. Gwebu, T. Matthews, et al., Nanomaterials 11 (2021) 34685167.
[32] J. Xu, Z. Wei, S. Zhang, et al., J. Colloid Interface Sci. 588 (2021) 378–383.
[33] K. Zhang, C. Wang, D. Bin, et al., Catal. Sci. Technol. 6 (2016) 6441–6447.
[34] J. Liu, Z. Luo, J. Li, et al., Appl. Catal. B 242 (2019) 258–266.
[35] N.T.N. Anh, A.D. Chowdhury, Sens. Actuator. B: Chem. 252 (2017) 1169–1178.
[36] S. Zhao, M. Lan, X. Zhu, et al., ACS Appl. Mater. Interfaces 7 (2015) 17054–17060.
[37] S.W. Koh, J. Hu, H. Chun, ACS Appl. Mater. Interfaces 14 (2022) 12156–12167.
[38] X. Wang, H. Gao, C. Zhai, et al., Ind. Eng. Chem. Res. 59 (2020) 19252–19259.
[39] H. Zhang, C. Zhai, P. Yang, et al., Energy Technol. 8 (2019) 1900731.
[40] H. Xu, P. Song, C. Fernandez, et al., J. Taiwan Inst. Chem. Eng. 91 (2018) 316–322.
[41] H. Gao, C. Zhai, C. Yuan, et al., Electrochim. Acta 330 (2020) 135214.
[42] H. Feng, Y. Chen, R. Wang, Chin. Chem. Lett. 33 (2022) 1117–1130.
[43] J. Wang, J. Pei, W. Liu, Chin. Chem. Lett. 34 (2023) 108157.
[44] H. Xu, B. Yan, K. Zhang, et al., Int. J. Hydrogen Energ. 42 (2017) 11229–11238.
[45] Y. Gong, J. Wang, Z. Cheng, Chin. Chem. Lett. 34 (2023) 107535.